The Influence of Leading-edge Tubercles on the Hydrodynamic Performance and Propeller Wake Flow Development of a Ducted Propeller

Callum Stark, Weichao Shi
Naval Architecture and Ocean Marine Engineering Department, University of Strathclyde
Glasgow, UK

ABSTRACT

This study implements leading-edge (LE) tubercles on a benchmark 19A accelerating duct to investigate the impact on the hydrodynamic performance and propeller wake flow development at multiple operating conditions. The study was conducted using Computational Fluid Dynamics (CFD) where the sliding mesh technique was used to describe the propeller rotation and the hydrodynamic flow-field was solved using Improved Delayed Detached Eddy Simulations (IDDES). In summary, it was found that LE tubercles can enhance the thrust of the duct by a maximum of 7.15% and disrupt the coherent vortex structure of the benchmark ducted propeller which will likely influence the noise signature of the propulsor.

KEY WORDS: Leading-edge tubercles; biomimetics, ducted propeller; CFD; wake dynamics

INTRODUCTION

Shipping, which is a relatively environmentally friendly mode of transport, is the dominant and will remain the most important transport mode for world trade. However, the shipping industry consumes more fuel in comparison with other transport modes and shipping-related emissions contribute significantly to the global air pollution and long-term global warming which is increasing at an alarming rate (Wan et al. , 2016). Therefore, reducing fuel consumption will not only save the ship owners money, but assist in the worldwide target to reduce the rate at which global warming is increasing. In addition, the rate at which ambient ocean levels are increasing is a concern amongst the maritime community, where anthropogenic noise has a negative impact on marine creatures who utilise the underwater acoustic environment to perform basic living functions such as navigating and catching prey, This has resulted in international bodies such as the International Maritime Organization (IMO) publishing non-mandatory guidelines to reduce ambient ocean noise levels (IMO., 2014). Within the maritime sector, improving the hydrodynamic and hydroacoustic performance of marine propulsors is an area which can significantly reduce fuel consumption, carbon emissions and noise signature from marine craft. In order to achieve this, one can look to mother nature for inspiration as humankind has done so many times in order to answer our problems.

Ironically, a marine mammal that is negatively impacted by the by-products of marine vessels is the inspiration behind this biomimetic research. The humpback whale is a magnificent creature that despite its large and cumbersome build, can catch prey using acrobatic, agile maneuvers. These maneuvers are made possible because of the small bumps located on the pectoral fin and are known as leading-edge (LE) tubercles. This concept has been the focus of numerous studies over the last few decades on a multitude of applications to understand the influence on the flow-field, how these bumps benefit the humpback whale and how it can benefit the performance of human-made devices. This plethora of research was initiated by Watts and Fish., (2001) where a panel code method was used to determine the fundamental fluid dynamics of LE tubercles on a airfoil. They found a 4.8% increase in lift, a 10.9% reduction in induced drag, and a 17.6% increase in lift to drag ratio at 10^0 angle of attack at a large Reynolds number. It was stipulated that the LE tubercles would influence the flow separation and post-stall regime. This was further confirmed when Miklosovic et al., (2004) conducted experimental tests in a wind tunnel on a model scale humpback whale flipper with and without LE tubercles. It was shown

that the addition of leading-edge tubercles to a scale model of an idealised humpback whale flipper delays the stall angle by approximately 40%, while increasing lift and decreasing drag. The LE tubercle effect was likened to vortex generators that energise the flow over an aircraft wing, stipulating that the performance gain in the post-stall regime was attributed to the generation of vortex structures that energise the boundary layer and encourage flow attachment which would not be possible without such a feature.

Since then, the concept has been studied on a variety of marine applications such as hydrofoils, marine control surfaces such as rudders and tidal turbines. Johari et al., (2007) conducted experimental research on hydrofoils in a water tunnel on leading-edge tubercles at a high Reynolds number while varying the amplitude and wavelength of the idealised sinusoidal waveform. It was noted that post-stall life increased up to 50% with only ever a slight compromise in induced drag. Additionally, there was an increase in drag and reduction in lift in the pre-stall region. In terms of the sinusoidal geometrical parameters, it was shown that amplitude had a much more significant effect on the performance of the hydrofoil compared to the wavelength, which had very minimal influence. Marine control surfaces such as rudders have also been the benefactors of LE tubercle research. Weber et al., (2010) used experimental methods to investigate the effect of LE tubercles on the lift, drag and cavitation onset operating at low Reynold's numbers. It was concluded that the inclusion of LE tubercles accelerated the onset of cavitation. At angles of between 15 and 22^0 in the lower Reynolds numbers, LE tubercles increased drag and reduced lift, but at angles of above 22^0, the LE tubercles improved the lift capability of the rudder. At the higher Reynolds numbers, the difference in performance between the smooth LE and tubercle LE was negligible, therefore suggesting there is a critical Reynold's number to which a LE tubercle configuration can affect the hydrodynamic performance. Shi et al., (2016a, 2016b, 2017) established the concept onto the tidal turbine. An in-depth numerical and experimental study was conducted into the feasibility of LE tubercles on such a device. The study showed an improvement in power coefficient at low tip speed ratios, containment of cavitation and reduction of underwater radiated noise in some operating conditions. It was found that the inclusion of LE tubercles resulted in an earlier inception of cavitation, but in heavier cavitating conditions the cavitation was restricted to the troughs of the tubercles, similar findings to Weber et al., (2010).

In summary, the LE tubercle concept has proven to bring hydrodynamic performance improvement in certain operating conditions for several different marine applications and this could be similar for other marine applications yet to be trialed with LE tubercles. To the author's knowledge, LE tubercles have not been applied to the duct of the ducted propeller. This study aims to use high-fidelity DES to understand the influence on global hydrodynamic performance and how the implementation of LE tubercles can influence and disrupt the coherent vortex structure produced by the ducted propeller which could affect the resulting noise signature.

NUMERICAL APPROACH

Commercial code STAR CCM+ was used to complete this study. Firstly, incompressible steady Reynolds-averaged Navier Stokes (RANS) solver using the popular SST k-omega turbulence model and moving reference frame (MRF) methodology was used. This was then compared to experimental data for validation. The steady-MRF method is well-known for providing accurate hydrodynamic performance prediction at a significantly reduced computational cost when compared to the unsteady Rigid Body Motion (RBM) method (Sezen et al. 2020). The steady MRF method is a time-averaged approach where the propeller is fixed and the rotating region adopts a local frame of reference to rotate the fluid, whereas the RBM method requires transient analysis as the rotating propeller is moved a fixed displacement per time step, more commonly known as the sliding mesh technique. The rotation rate was fixed at 15rps and the advance velocity was varied to predict the open-water curve characteristics. The Reynold's number was estimated as 1.05×10^6 based on the rotational rate.

However, in order to improve the prediction of the propeller wake flow, implicit unsteady DES was used to solve the hydrodynamic flow-field and the Rigid Body Motion (RBM) method was used to model the propeller revolutions. The specific formulation of DES used was the Improved Delayed Detached Eddy Simulation (IDDES), this solves the near-wall regions using a RANS approach, in this case using the SST k-omega turbulence model, with the large eddy simulation (LES) solver used to solve the rest of the domain. DES was used as oppose to RANS as it has been shown that the RANS solver does not capture the instabilities within the propeller wake flow (Guilmineau et al., 2014), and in the case of tubercles, the suitability of the RANS solver has been questioned, especially in flow separation conditions (Weber et al., 2011).

The RBM method was also selected to model the propeller revolutions for the study of the propeller slipstream, more commonly known as the sliding mesh technique. RBM is considered the most accurate methodology to predict unsteady propeller flow (Sezen and Kinaci., 2019), where a time-step of 1 degree of rotation per time-step was selected which is roughly 1.85e-4s. Y+ <1 was used with a low wall y+ treatment which assumes that the boundary layer is resolved by the near-wall mesh. The second order scheme was applied to the temporal discretisation. The ducted propeller ran for 15 revolutions using the RBM method, where hydrodynamic variables had converged, and the propeller wake flow had developed sufficiently downstream.

TEST CASE

Overview

The reference geometry 'REF' was selected as the benchmark 19A ducted propeller and Kaplan series, KA4-55 propeller, detailed geometry can be found in (Carlton 2018). The rendered geometry can be found in Fig. 1a and the parameters in Table 1.

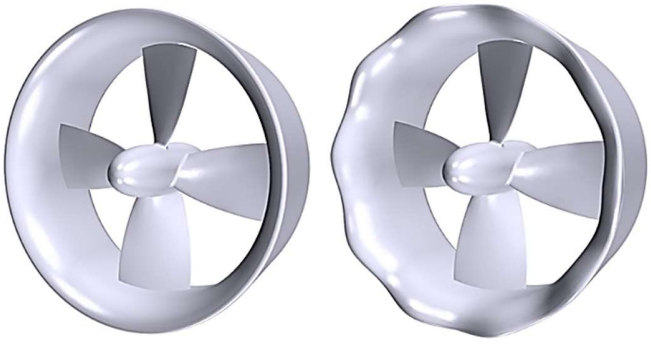

a) REF b) SLE

Fig. 1 Ducted propeller geometry

Table 1 Geometrical parameters of reference ducted propeller

Variable (Duct)	**Unit**	**Variable (Propeller)**	**Unit**
Type	19A	**Type**	Kaplan
Outer Diameter, D_d	0.306m	**Blade Number**	4

Inner Diameter, D_i	0.254m	**Expanded Area Ratio (EAR)**	0.55
Duct Chord, L_{DUCT}	0.125m	**Pitch-diameter Ratio (P/D)**	1
		Diameter, D	0.25m
		Tip Clearance, t	2mm
		Position wrt Duct	$0.5L_{DUCT}$

The tubercle duct was created as an idealised sinusoidal waveform with an amplitude of 5mm (A/L_{DUCT}=0.05) and a tubercle count of 10 (λ/L_{DUCT} = 0.75), labelled as 'SLE' duct. The 3D design can be shown in Fig. 1b. The geometrical parameters of the tubercle were selected based on a previous unpublished optimisation study where several amplitude and wavelength configurations were investigated.

Computational Domain

The computational domain consisted of a cylindrical domain, where the propeller was located 3D from the inlet and 8D from the outlet and 2.5D from the outer circumferential wall. The inlet was defined as a velocity inlet, outlet as pressure outlet and symmetry plane on the circumferential face as shown in Fig. 2. The rotating domain of the propeller and static region of the surrounding volume were separated by an internal interface. The duct and propeller were defined as non-slip walls.

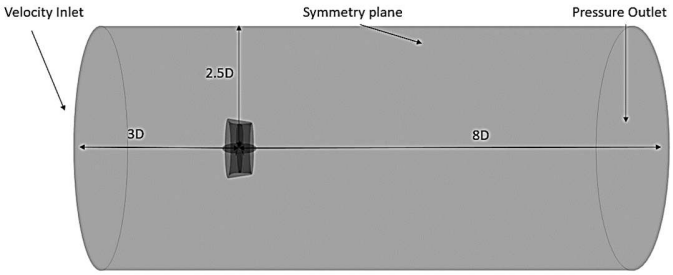

Fig. 2 Computational domain

Mesh Generation

The mesh was generated using unstructured hexahedral mesh to the count of approximately 13 million cells, where prism layers were used to resolve the boundary layer. A low Y+ wall approach was employed, where the average Y+ <1, with a maximum of roughly 2.3 located on the blade leading-edge. An interface prism layer between the rotating region of the propeller and the surrounding static region was created to ensure mesh alignment between regions. A volumetric control was selected to maintain a uniform mesh in a section of the propeller slipstream of interest. Although the mesh structure may agree well with experimental hydrodynamic variables, the wake flow field does not need to be resolved sufficiently for this to be achieved. Resolving the wake flow is crucial to understand the different vortex mechanisms occurring in the slipstream and therefore, the mesh structure must be suitable to allow this. Further volumetric controls were applied to allow smooth transition to the core mesh. The blade and duct surface mesh can be shown in Fig. 3 and a section of volume mesh shown in Fig. 4.

a) Propeller mesh b) REF duct mesh

Fig. 3 Surface mesh of the propeller and REF duct

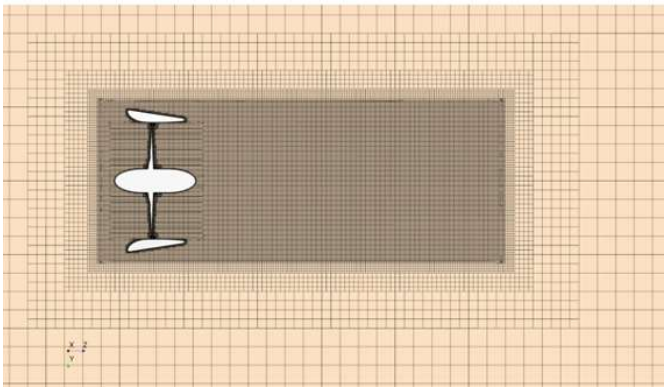

Fig. 4 Cut plane volume mesh of computational domain

VERIFICATION AND VALIDATION

Performance Coefficients

The hydrodynamic performance of the ducted propeller was predicted using the traditional open-water characteristics. Ducted propeller performance coefficients can be outlined in Eqns. 1-6.

$$K_{TP} = \frac{T_P}{\rho n^2 D^4} \quad (1)$$

$$K_{TD} = \frac{T_D}{\rho n^2 D^4} \quad (2)$$

$$K_{TT} = K_{TP} + K_{TD} \quad (3)$$

$$K_Q = \frac{Q}{\rho n^2 D^5} \quad (4)$$

$$ETA = \frac{K_{TT} J}{2\pi K_Q} \quad (5)$$

$$J = \frac{V_A}{nD} \quad (6)$$

Where K_{TP} is propeller thrust coefficient, K_{TD}, is duct thrust coefficient, K_{TT} is total duct thrust coefficient, $10K_Q$, is the torque coefficient and ETA, is open-water efficiency. Advance ratio, J, is defined by advance velocity V_A (m/s), n, rotation rate (rps) and propeller diameter D (m) and can be shown in Eqn. 6. T_P and T_D are propeller and duct thrust (N) respectively, Q is propeller torque (Nm) and ρ, is density (kg/m3).

Mesh Convergence Study

A verification study was conducted to determine the uncertainty of the numerical simulations. This was completed using the grid convergence (GCI) method first proposed by Roache., (1998) and based on Richardson., (1911) and is also recommended in the ITTC procedure (ITTC., 1999). The full methodology implemented in this study was defined by Celik et al., (2008) and can be found within. The total thrust and torque coefficient (K_{TT} and $10K_Q$) were selected as the integral variable at advance ratio, J=0.55, the operating condition at which maximum efficiency is achieved. The tabulated results can be shown in Table 2.
The difference between the solution scalars (ε) should be determined by Eqn. 7.

$$\varepsilon_{21} = \varphi_2 - \varphi_1, \quad \varepsilon_{32} = \varphi_3 - \varphi_2, \tag{7}$$

where, φ_1, φ_2 and φ_3 represent the results using fine, medium and coarse mesh grids, respectively. The cell counts for the fine, medium and coarse mesh were 13, 7 and 3 million, respectively. The ratio of solution scalars is used to calculate the convergence condition by Eqn. 8.

$$R = \frac{\varepsilon_{21}}{\varepsilon_{32}} \tag{8}$$

Solution type is determined with respect to the convergence condition, R: 1. oscillatory convergence, -1<R<0; 2. monotonic convergence 0<R<1; 3. oscillatory divergence R<-1; and 4. monotonic divergence, R>1, If R is found as in case 2, the procedure can be directly employed. GCI index is calculated by the following in Eqn. 9:

$$GCI_{fine}{}^{21} = \frac{1.25 e_a{}^{21}}{r_{21}{}^{p} - 1} \tag{9}$$

Here, p is apparent order, e_a is an approximate relative error. Detailed information about the verification procedure can be found in Celik et al. (2008). Results obtained for the total thrust and torque coefficient and uncertainty level are given in Table 2. As shown, the convergence condition R, was between 0 and 1 (monotonic convergence). As a result of the uncertainty study at J=0.55, the fine mesh was selected, where a range of operating conditions were considered.

Table 2 Uncertainty result for K_{TT}

	φ_1	φ_2	φ_3	R	%GCI_{FINE}
K_{TT}	0.178	0.177	0.172	0.13	0.23
$10K_Q$	0.279	0.278	0.276	0.33	0.83

Hydrodynamic Validation with Experimental Test

By comparing experimental data acquired during an internal test campaign using a KA4-55 and 19A duct conducted at CTO, the numerical methodology was validated. The description of the geometry can be shown in Table 1 and was replicated in the computational domain.

Fig. 5 shows the results acquired, where advance ratios ranging from 0.001 to 0.7 were considered. As can be seen, the computational environment generated can be used to determine the open water characteristics of the ducted propeller selected in this study to within a good degree of accuracy, with relative errors of total thrust and torque coefficient; 5.1 and 1.4% respectively.

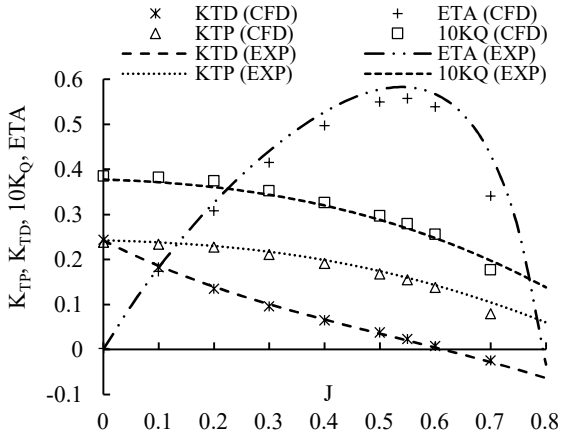

Fig. 5 KA4-55 + 19A duct validation with experimental test

RESULTS AND DISCUSSIONS

Global Performance Results and Analysis

Fig. 6 shows the percentage difference (Δ%) of key time-averaged global performance coefficients for the SLE ducted propeller combination when compared to REF using the sliding mesh technique and DES solver at a range of operating conditions. As can be seen, the duct performance can be enhanced by a maximum of 7.15% at the maximum operating efficiency, increasing the optimum efficiency by roughly 0.55%. It appears that at J = 0.5 and 0.6, there is performance degradation due to the inclusion of tubercles. This is likely due to earlier-inception of flow separation occurring in the troughs at J = 0.5, and the geometrical configuration of tubercles not being prominent enough to manipulate the flow at J=0.6 which will be explained with further analysis. Nonetheless, in between these flow separation conditions, the tubercles can enhance the performance of the duct. Additionally, the LE tubercles result in a reduction of propeller thrust and torque. Therefore, the LE tubercles must influence the inflow characteristics of the propeller.

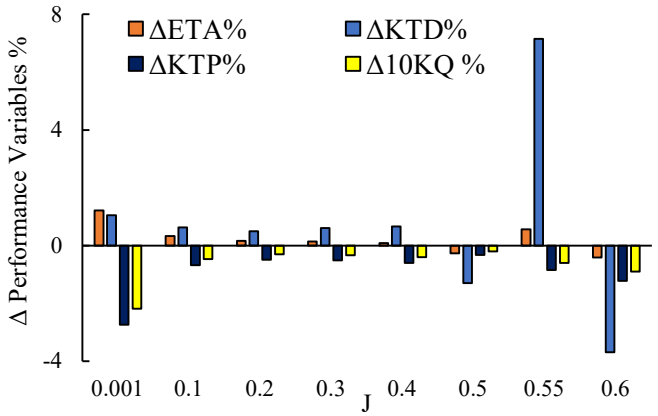

Fig. 6 Δ% of key performance variables when compared to REF at a range of J.

Propeller Inflow Characteristics

Fig. 7 shows the velocity vector plots for each condition of the REF duct, showing as J is increased, the negative angle of attack is reduced. The duct thrust is created by the difference in horizontal component of lift and drag which varies with J. The pressure and streamwise vorticity inflow characteristics for SLE and REF ducts at $0.26L_{DUCT}$ from the leading-edge of the REF duct or the trough leading-edge section of the SLE duct at an example advance ratio, J = 0.55 can be shown in Fig. 8. As can be seen, the LE tubercles influence the propeller inflow characteristics, this is likely the reason for the variation in blade thrust and torque. Although there is no appreciable difference in pressure distribution, the tubercles create the contra-rotating streamwise vortices on the suction side of the duct which will interact with the blade surface near the duct wall. The variation in blade thrust and torque with J number is likely due to the strength of the streamwise vortices varying because the inflow angle will change with the advance ratio.

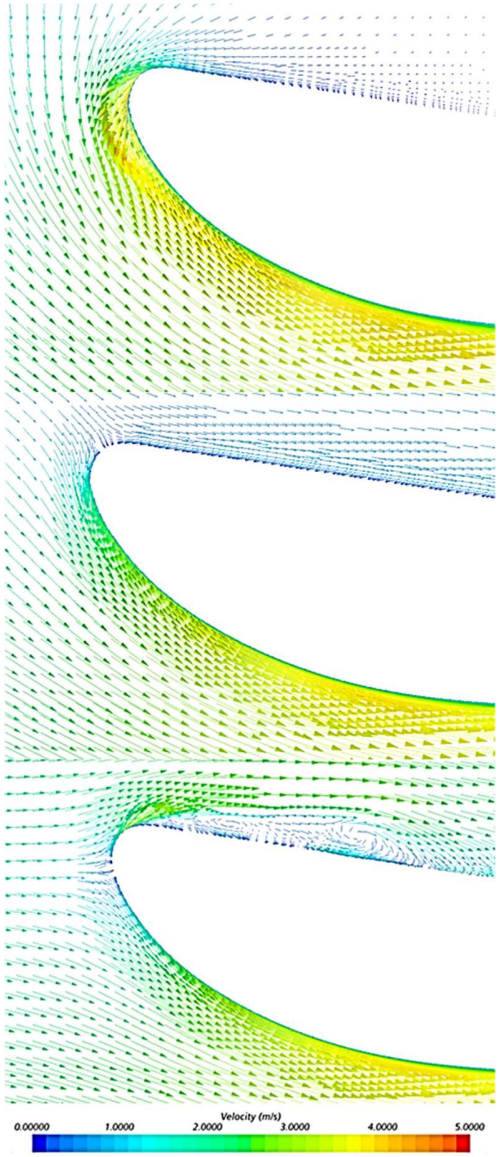

Fig. 7 Inflow angle with varying J, 0.1 (top), 0.3 (middle) and 0.55 (bottom) respectively.

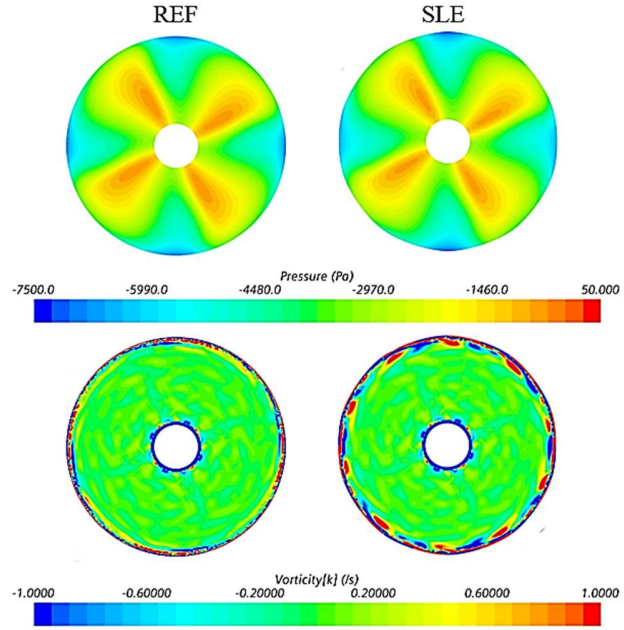

Fig. 8 Inflow pressure and streamwise vorticity characteristics at $0.26L_{DUCT}$ for both REF and SLE ducts at J = 0.55

Pressure and Velocity Distributions

The distribution of pressure on the SLE and REF duct surface (suction side) at J = 0.1, 0.3 and 0.55 can be shown in Fig. 9. On the suction side of the blade tip a low-pressure area can be observed which is caused by a vortex that is formed by the rotation of the blade close to the duct wall and is known as a tip-leakage vortex. This type of vortex has a pitch that is considerably lower than the pitch of the blade. The high-low pressure pattern created by the inclusion of the tubercles at the leading-edge can be seen more prominently at the heavier-loaded condition, J = 0.1. At this condition, the duct experiences a high negative angle of attack with respect to the incoming flow. Downstream of the blade, a pressure trail can be shown in all configurations which can be described as the development of the tip-leakage vortex into the propeller slipstream. The inclusion of the LE tubercles can be seen to disrupt this vortex, creating fluctuations in the pressure trail, particularly at the lower J ratio.

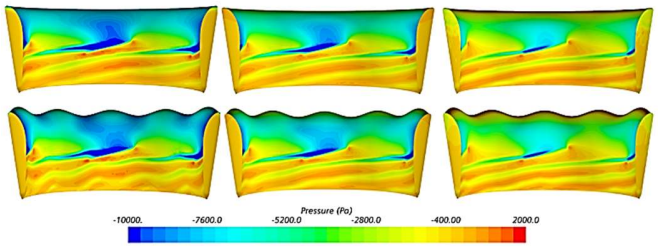

Fig. 9 Surface pressure distributions (suction side) of REF and SLE duct at J = 0.1 (left), 0.3 (middle) and 0.55 (right)

Fig. 10 displays the differences in surface pressure distribution incurred by the inclusion of the LE tubercles on the pressure side of the duct at J = 0.3, 0.5, 0.55 and 0.6 and the velocity of the flow-field at cut planes along the trough and peak sections of the SLE duct. It can be shown that no flow separation is experienced at J = 0.3, therefore the improvement in duct thrust may be due to the additional lift producing surface area of

the tubercle and the low-high pressure pattern on the suction side of the duct. At J = 0.5, the flow separation is initiated earlier behind the troughs of the tubercle than compared to REF duct. This results in a likely increase in drag which would correspond to the degradation in performance at this condition. At J = 0.55, the isolation of flow separation can be shown behind the troughs, with flow attachment behind the peaks, compared to spanwise flow separation of the REF duct, this corresponds to a 7.15% improvement in duct thrust at this condition. At J = 0.6, the SLE duct does not appear to be able to manipulate the flow at this condition, showing flow separation behind the peaks and troughs, this is likely due to the geometrical configuration of the tubercle not being prominent enough.

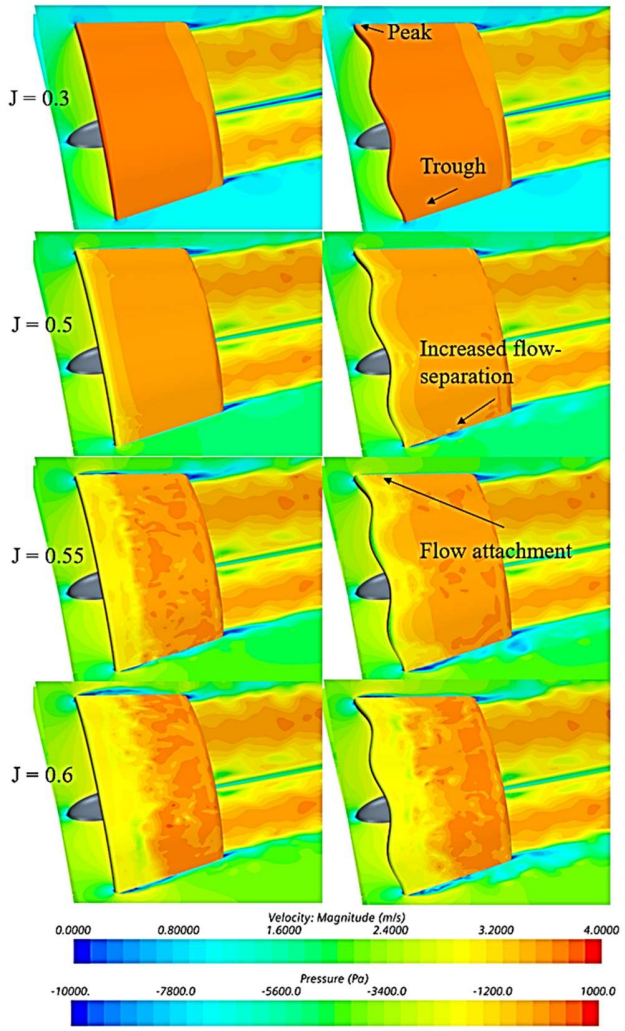

Fig. 10 Duct surface pressure distributions (pressure side) and velocity distributions of REF and SLE duct at J =0.3, 0.5, 0.55 and 0.6 respectively.

Surface Streamwise Vorticity Distribution

Fig. 11 shows the surface streamwise vorticity displayed on the ducted propeller at operating conditions J = 0.1, 0.3 and 0.55. At all operating conditions, counter-rotating streamwise vortices on the suction side of the duct can be observed. Where flow separation occurs on the pressure side of the duct at J = 0.55, a vorticity funneling pattern can be seen behind the troughs with no vorticity present behind the peaks. This can be compared with the reference design at the same condition, where scattered vorticity can be displayed along the spanwise direction of the duct. Comparing the vortex pair generated at J = 0.1 to 0.3 and 0.55, the streamwise vortices are less distinct at the heavier-loaded condition.

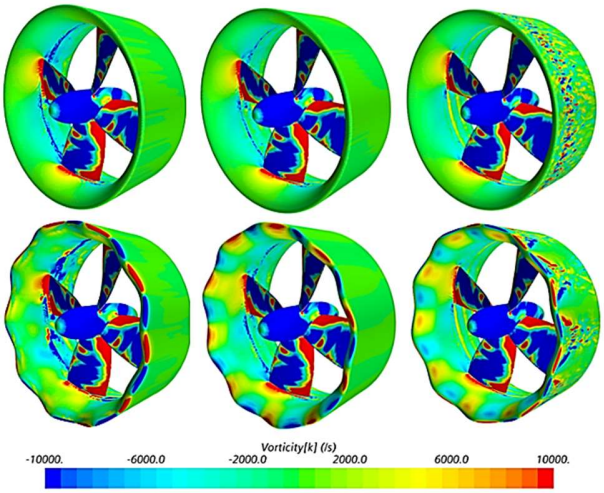

Fig. 11 Surface streamwise vorticity distributions of REF and SLE duct at J = 0.1 (left), 0.3 (middle) and 0.55 (right)

Propeller Wake Flow Analysis

Turbulent Kinetic Energy (TKE) surface integrals for 7 cross-sections downstream of the ducted propeller for both REF and SLE were computed. Comparing the SLE to the REF duct, there was a reduction in TKE at the further downstream sections for all operating conditions considered as shown in Fig. 12. Fig. 12 shows the percentage reduction of computed surface integral TKE at several plane sections for the 3 operating conditions considered, where the positive y-axis denotes a reduction in TKE. The SLE duct initially increases the TKE in the propeller wake but dissipates quicker than the REF duct for all operating conditions further downstream. A maximum of 16% reduction in TKE is observed at J = 0.1.

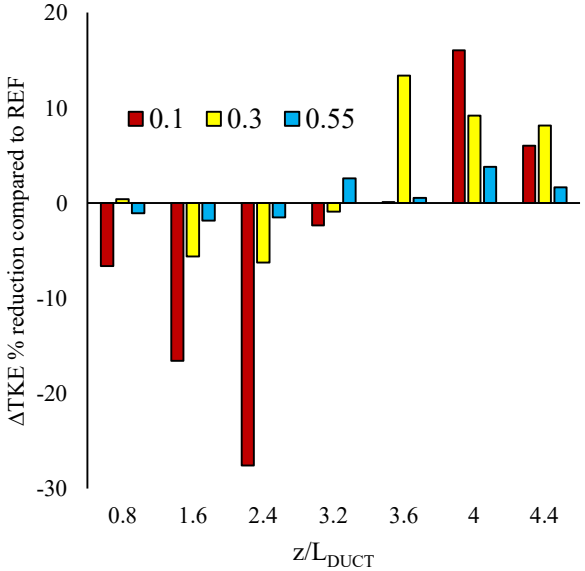

Fig. 12 TKE reduction (denoted as positive y-axis) of SLE duct compared to REF at several positions in the propeller slipstream for J = 0.1, 0.3 and 0.55, respectively.

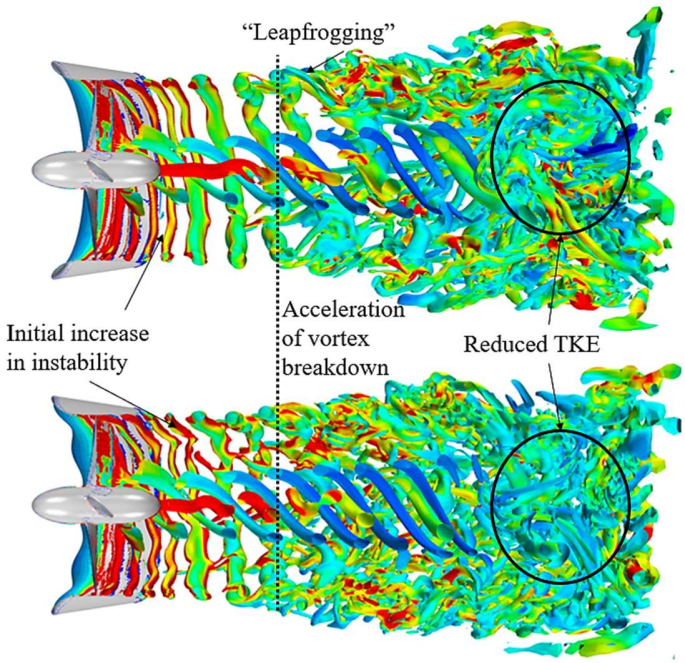

a) J = 0.1

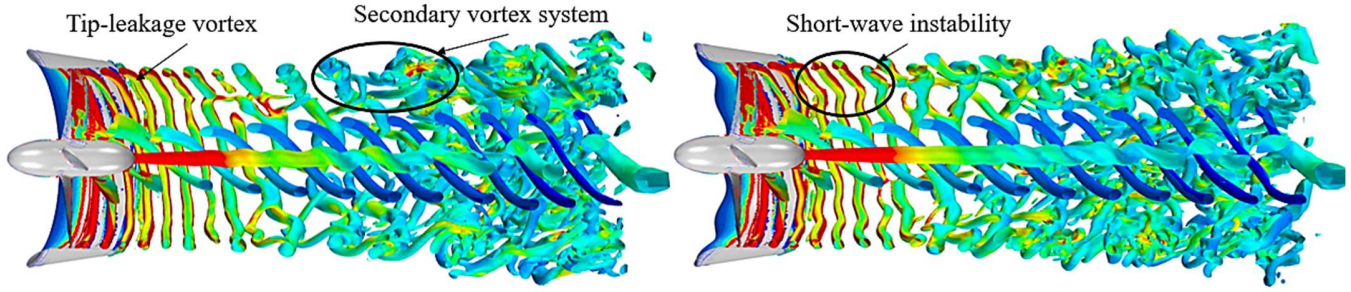

b) J = 0.3

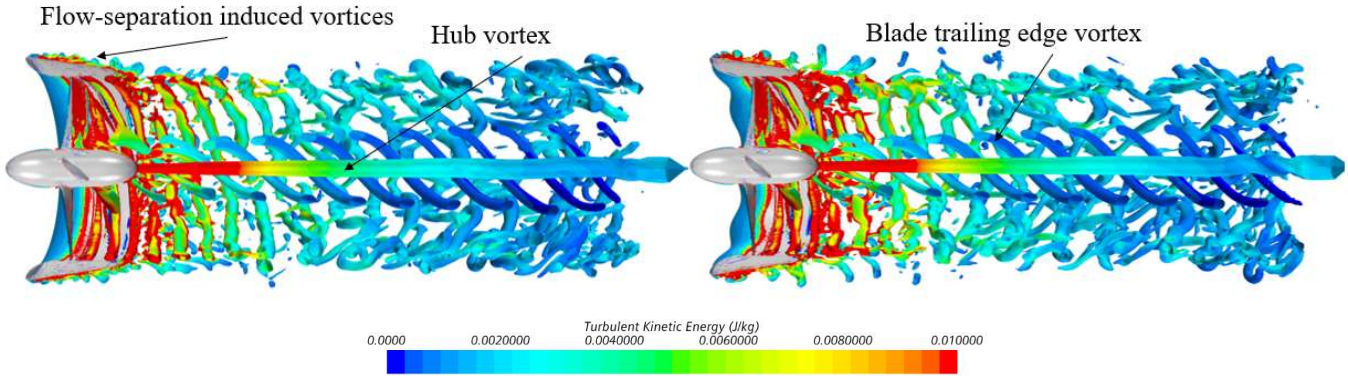

c) J = 0.55

Fig. 13 Q-criterion plots (right), $\alpha = 1000/s^2$ (coloured by TKE) of REF and SLE ducts at J = 0.1, 0.3 and 0.55

Fig. 13 shows the instantaneous half-section Q-criterion plots of the propeller wake coloured by TKE at J = 0.1, 0.3 and 0.55 for the REF and SLE ducted propeller combinations. The helical vortex structure known as the tip-leakage vortex created by the rotation of the propeller and interaction with the duct wall, blade trailing edge vortex, hub vortex and "leapfrogging" vortex phenomenon can be observed and are highlighted. The short-wave instability within the helical vortex structure and the secondary vortex system can also be shown and highlighted. At J = 0.55, the flow-separation induced vortex structure can be observed over the pressure side of the duct. At the operating condition where the blade loading is the highest (J = 0.1), the tip-leakage vortex breaks down a lot quicker downstream when compared to the lower blade loading (J = 0.3, 0.55) where the delayed breakdown in the tip-leakage vortex structure can be shown. In addition, at J = 0.1, the earlier breakdown of the vortex structure leads to a larger distribution of TKE further downstream. The primary mechanism for the breakdown of the tip-leakage vortex observed is the short-wave instability, followed by the secondary vortex system. Similar findings were observed by Zhang and Jaiman., (2019) where the stability and breakdown of a helical vortex structure is further explained by Widnall., (1972). As can be seen, the SLE duct influences the wake dynamics of the ducted propeller when compared to the REF. Immediately at the exit of the ducted propeller, the inclusion of the LE tubercles appear to create additionally instability within the helical tip-leakage vortex structure. At J = 0.1, this leads to an acceleration in the vortex breakdown into large-scale flow structures and turbulence.

CONCLUSION

This study showed the effect of the implementation of LE tubercles on the hydrodynamic performance and the wake structure on marine ducted thrusters using IDDES. The fundamental tubercle mechanisms were identified, namely the streamwise counter-rotating vortices, high-low pressure patterns at the leading-edge and the compartmentalisation of flow separation when flow separation occurs.

It has shown that the inclusion of LE tubercles can improve the duct thrust performance by a maximum of approximately 7.15% and an improvement of optimum propulsive efficiency to a maximum of approximately 0.55%. But this is also due to the influence of LE tubercles on the propeller blades, which reduce the propeller thrust and torque coefficient. The impact on the blade performance is likely due to the interaction between the blade and the induced streamwise vortices of the SLE duct and will vary with the strength of the vortex pairs. The strength of the vortex pairs induced will change at different J due to the varying inflow angles experienced. In addition, the inclusion of LE tubercles changes the wake dynamics of the ducted propeller particularly in the lower advance ratio J = 0.1. It was shown that the SLE duct increases the instability of the initial tip leakage vortex, which accelerates the breakdown of the vortex structure and ultimately, reduces the turbulent kinetic energy further downstream at J = 0.1. This is most likely due to the addition of the streamwise vortex pairs into the propeller inflow which will create additional instabilities within the helical tip-leakage vortex.

Further work will aim to use the Ffowcs Williams-Hawkings (FW-H) acoustic analogy to predict the influence of LE tubercles on the far-field noise from the ducted propeller. The variation in propeller wake structure will likely influence the turbulence and vorticity induced noise signature.

ACKNOWLEDGEMENTS

Results were obtained using the ARCHIE-WeSt High-Performance Computer (www.archie-west.ac.uk) based at the University of Strathclyde. The funding support from BAE systems plc. is greatly appreciated and acknowledged (Ref: MEIR PhD 16).

REFERENCES

Carlton, J. (2018). *Marine propellers and propulsion*. Butterworth-Heinemann.

Celik, I. B., Ghia, U., Roache, P. J., & Freitas, C. J. (2008). "Procedure for estimation and reporting of uncertainty due to discretization in CFD applications," *Journal of Fluids Engineering-Transactions of the ASME*, 130(7).

Guilmineau, E., Deng, G. B., Leroyer, A., Queutey, P., Visonneau, M., & Wackers, J. (2014). "Wake simulation of a marine propeller," *In 11th World Congress on Computational Mechanics (WCCM XI), 5th European Conference on Computational Mechanics (ECCM V), 6th European Conference on Computational Fluid Dynamics (ECFD VI), July (Vol. 20).*

IMO. (2014). "Guidelines for the reduction of underwater noise from commercial shipping to address adverse impacts on marine life."

ITTC. (1999). "ITTC–recommended procedures," *In International Towing Tank Conference.*

Johari, H., Henoch, C., Custodio, D., & Levshin, A. (2007). "Effects of leading-edge protuberances on airfoil performance," AIAA Journal, 45(11), 2634-2642.

Miklosovic, D. S., Murray, M. M., Howle, L. E., & Fish, F. E. (2004). "Leading-edge tubercles delay stall on humpback whale (Megaptera novaeangliae) flippers," *Physics of Fluids,* 16(5), L39-L42.

Richardson, L. F. (1911). IX. "The approximate arithmetical solution by finite differences of physical problems involving differential equations, with an application to the stresses in a masonry dam," *Philosophical Transactions of the Royal Society of London. Series A, Containing Papers of a Mathematical or Physical Character*, 210(459-470), 307-357.

Roache, P. J. (1998). "Verification of codes and calculations," *AIAA Journal*, 36(5), 696-702.

Sezen, S., Atlar, M., Fitzsimmons, P., Sasaki, N., Tani, G., Yilmaz, N., & Aktas, B. (2020). "Numerical cavitation noise prediction of a benchmark research vessel propeller," *Ocean Engineering*, *211*, 107549.

Sezen, S., & Kinaci, O. K. (2019). "Incompressible flow assumption in hydroacoustic predictions of marine propellers," *Ocean Engineering*, *186*, 106138.

Shi, W., Atlar, M., Rosli, R., Aktas, B., & Norman, R. (2016). "Cavitation observations and noise measurements of horizontal axis tidal turbines with biomimetic blade leading-edge designs," *Ocean engineering*, *121*, 143-155.

Shi, W., Rosli, R., Atlar, M., Norman, R., Wang, D., & Yang, W. (2016). "Hydrodynamic performance evaluation of a tidal turbine with leading-edge tubercles," *Ocean Engineering*, *117*, 246-253.

Shi, W., Atlar, M., Norman, R., Aktas, B., & Turkmen, S. (2016). "Numerical optimization and experimental validation for a tidal turbine blade with leading-edge tubercles," *Renewable Energy*, *96*, 42-55..

Shi, W., Atlar, M., & Norman, R. (2017). "Detailed flow measurement of the field around tidal turbines with and without biomimetic leading-edge tubercles," *Renewable Energy*, *111*, 688-707.

Wan, Z., Zhu, M., Chen, S., & Sperling, D. (2016). "Pollution: Three steps to a green shipping industry," *Nature*, *530*(7590), 275-277.

Watts, P., & Fish, F. E. (2001, August). "The influence of passive, leading edge tubercles on wing performance," In *Proc 12th Internat Symp Unmanned Untethered Submersible Tech. Durham, NH: Autonomous Undersea Systems Institute*.

Weber, P. W., Howle, L. E., & Murray, M. M. (2010). "Lift, drag, and cavitation onset on rudders with leading-edge tubercles," *Marine technology*, *47*(1), 27-36.

Weber, P. W., Howle, L. E., Murray, M. M., & Miklosovic, D. S. (2011). "Computational evaluation of the performance of lifting surfaces with leading-edge protuberances," *Journal of Aircraft*, *48*(2), 591-600.

Widnall, S. E. (1972). "The stability of a helical vortex filament," *Journal of Fluid Mechanics*, *54*(4), 641-663.

Zhang, Q., & Jaiman, R. K. (2019). "Numerical analysis on the wake dynamics of a ducted propeller," *Ocean Engineering*, *171*, 202-224.